Multi-tuned RF Coil using Microfluidically Tunable RF Capacitor for MRI/MRS at 7T

Ashraf Abuelhaija[1], Sanaa Salama[2], Mohammed El-Absi[3]

Abstract – *Multi-nuclear magnetic resonance imaging and spectroscopy are considered valuable tools due to their capability of diagnosis and monitoring of several diseases. They require multi-nuclear RF coils to interrogate the proton (^1H) and other nuclei (X-nuclei) in the human body. Such coils provide anatomical images by acquiring (^1H) spectra and metabolities information by acquiring spectra of X-nuclei. In addition, the high signal received from proton (^1H) is used for B_0 shimming purposes. However, the signal strength for these X-nuclei is too low. Hence, the signal-to-noise-ratio (SNR) is low. The main advantages of using multinuclear RF coils are that they speed up the imaging process and reduce the spatial positioning error that might arise when replacing the RF coil in order to perform imaging of different nuclei. In addition, comfortable environment will be provided for patients by avoiding any inconvenience of moving out and asking to replace the coils. In this paper, a multi-tunable microstrip transmission line RF coil has been designed by using microfluidically tunable RF capacitor. This capacitor offers a wide range of capacitance tuning which extends between C_{min}=1.76 pF and C_{max}=48.7 pF. Hence, a wide range of resonant frequencies (f_{min}=75 MHz - f_{max}=298 MHz) can be offered by this coil to excite several nuclei at a field strength of 7T..*

***Keywords**: Magnetic Resonance Imaging (MRI), Magnetic Resonance Spectroscopy (MRS), Microstrip Transmission Line RF coil, Double-tuned (DT), Microfluidically Tuned Capacitor (μTC)*

I. Introduction

Magnetic resonance imaging and spectroscopy (MRI/S) are known as valuable and promising diagnostic tools because of their ability to investigate metabolism in human body such as ^{3}1P, ^{7}Li, ^{23}Na, ^{13}C, etc., which are called "x-nuclei". For example, 23Na MRI is used to quantify the glycosaminoglycan content in cartilage and therefore can detect and assess the biochemical degradation of cartilage in osteoarthritis. In addition, ^{23}Na MRI can be also used to detect brain tumours by showing the increase of sodium concentration in patient's brain relative to the structure of normal one [1]. Recently, ^{23}Na MRI has demonstrated diagnostic importance in benign and malignant breast tumors [2], acute and subacute stroke [3], detection of mild alzheimer disease [4], and functional imaging of the human kidney [5]. Meanwhile, 31P MRS can provide informations on muscle function [6], therefore patients who suffer from muscular disorder can perform clinical follow-up. ^{13}C MRS is used in metabolic studies such as measuring the rate of net hepatic glycogenolysis in humans [7]. Despite the low concentration of these nuclei in the body which leads to low signal strength (typically less than 1/1000 of ^{1}H) [8], several multinuclear MR applications have been demonstrated to provide biomedical information such as ^{1}H/^{23}Na [9–11], ^{1}H/^{13}C [12, 13] and ^{1}H/^{31}P [6, 14] spectroscopic imaging. Table 1 summarizes the gyromagnetic ratio and the resonant frequencies for ^{1}H and common.

Several techniques have been used to design and construct dual-tuned RF coils such as trap circuits [15] and PIN diodes [16]. These techniques employ lossy components which might lead to degrade the image quality.

In [17], a multi-tuned RF coil using variable capacitance diode (varactor) has been proposed. However, varactors have relatively high noise and low quality factor. An alternative variable capacitor which can be used is microelectromechanical system (MEMS) tunable capacitor. However, these capacitors suffer from low capacitance tuning range [18].

In this paper, a wide range of frequency tuning has been achieved by designing microfluidically tuned capacitors for meandered microstrip line RF coil at 7T.

II. DUAL-NUCLEI COIL METHODS

II.1. Double-Tuned RF Coil

This coil is designed to have capability of tuning at two-different frequencies: the proton frequency and the x-nuclei frequency. In [15], a double-tuned two-port surface RF coil for both ^{1}H- and ^{23}Na-MRI has been demonstrated. To achieve inter-channel decoupling, the designer has used trap circuit. A significant improvement

Manuscript received and revised xx 2010, accepted xx 2010

TABLE I
GYROMAGNETIC RATIO AND RESONANT FREQUENCY AT 7T FOR COMMON NUCLEI.

Nucleus	^{1}H	^{31}P	^{7}Li	^{23}Na	^{13}C
Gyromagnetic Ratio ($\gamma/2\pi$) in MHz/Tesla	42.6	17.2	16.5	11.3	10.7
Frequency @ 7T in MHz	298.0	120.6	115.8	78.8	75.0

in SNR has been achieved by this coil as well as optimal decoupling between both channels. In [19], a double-resonant $^{13}C/^{1}H$ surface coil system for in *vivo* application has been developed and implemented. In this design, specific filters have been implemented to decouple both channels. The double-tuned RF coil method has been applied for designing double tuning volume coil as well. For example, a low-pass birdcage coil has been designed for simultaneous acquisition of signal at two-frequencies (^{1}H and ^{31}P frequencies) by inserting trap circuits into its rungs [20]. Another demonstration of a double tuned birdcage RF coil using trap circuits has been presented in [21]. This coil has been designed for ^{23}Na and ^{1}H imaging at 1.5 Tesla. Another option to design a double tuned birdcage RF coil has been demonstrated in [17]. The designer has used variable capacitor (varactor) instead of trap circuit to tune between two-nuclei resonant frequencies at 3 Tesla for ^{19}F and ^{1}H imaging.

A wider frequency-switchable range technique has been proposed in [22]. This technique enable switching between 5 different frequencies by employing PIN diodes. A comparison between employing PIN diodes and trap circuits in designing dual-tuned RF coil has been intensively studied and presented in [23]. This study concludes that designing dual-tuned RF coil using PIN diodes offers lower losses and better tuning efficiency in comparison to trap circuits. However, a proposed solution to reduce the losses associated with trap circuits has been presented in [24] by improving the trap design.

II.2. Two separate RF Coils

This method requires two separate RF coils; one coil is tuned to the ^{1}H frequency and the other one is tuned to x-nuclei frequency. In order to obtain ^{1}H and x-nuclei images, either both coils are being used simultaneously or the imaging process is divided into two-phases; by obtaining each image individually. Coil exchange required extra scanning time in addition to the potential error which might arise due to repositioning the patient within the scanner. However, designers who use both coils simultaneously are required to suppress the interactions between coils.

Recently, several double-tuned RF coil designs that use two separate coils have been proposed. For example, in [25] a double-tuned RF surface coil to obtain ^{1}H and ^{23}Na images has been demonstrated. This double-tuned coil is comprised of a large square loop which has been tuned to ^{1}H frequency and a small square loop which has been tuned to ^{23}Na frequency. In order to suppress the interaction between the two loops, a trap circuit has been inserted in the small loop. In [26], 2 nested coaxial birdcage coil has been presented. This coil has been constructed by putting one of the birdcages inside the other. The inner birdcage (low-pass) has been tuned to the lower frequency and the outer birdcage (high-pass) has been tuned to the higher frequency. Alternatively, a folded four-ring quadrature birdcage coil has been designed as a double-tuned coil at 9.4T [27]. The outer coil (High-pass) has been tuned to ^{1}H frequency and the inner coil (low-pass) has been tuned to ^{23}Na frequency. This coil has demonstrated higher ^{23}Na image quality in comparison to the nested birdcage RF coils due to the improvement obtained in the SNR.

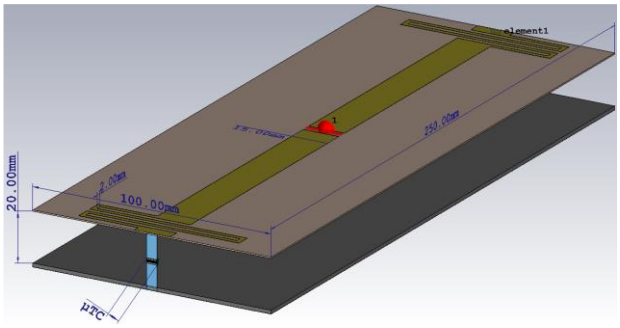

(a)

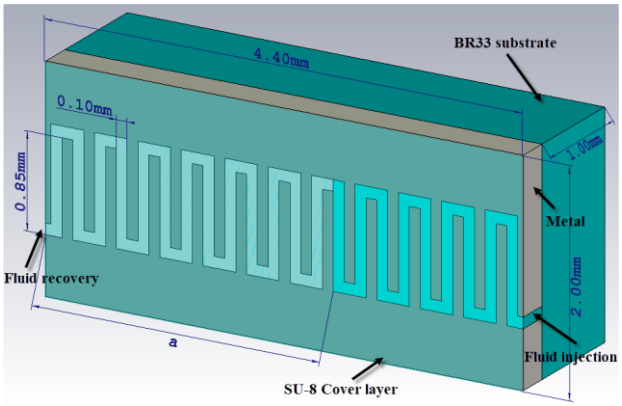

(b)

Fig.1. Multi-tunable microstrip transmission line RF coil. (a) Geometry of the meander RF coil. (b) The structure of microfluidically tuned capacitor.

In [28], a novel dual-tuned quadrature volume RF coil has proposed. This coil uses eight elements of half-wavelength ($\lambda/2$) microstrip RF coils for ^{1}H channel and eight elements of quarter-wavelength ($\lambda/4$) for 13C channel. The elements from the two types of RF coils have been arranged alternately along the circumference of a cylindrical volume. A homogeneous B_1 field at both resonant frequencies have been generated by the proposed design and high isolation between the two channels has been achieved. In [29], a hybrid technique of designing double-tuned RF coil at 7T has been proposed and

investigated. This design combines a microstrip transmission line RF coil and a lumped-element LC loop coil. The microstrip transmission line RF coil has been tuned to ^{1}H frequency whereas the lumped element loop coil has been tuned to ^{13}C frequency. This coil provides intrinsic decoupling between both coils due to the orthogonality of the magnetic fields from both coils.

III. MULTI-TUNABLE MICROSTRIP TRANSMISSION LINE RF COIL

III.1. Introduction to microstrip RF coil

In recent years, the demand of using ultra-high magnetic field MRI scanners has been increased for both clinical imaging and research studies. This is due to the achievements that have been obtained by these scanners in terms of high image quality and higher SNR [30–32]. In contrast, these scanners demand higher resonant frequency due to the increased operating magnetic field. The higher frequency requirement will increase the radiation losses as a consequence. To overcome this, challenge microstrip transmission line RF coils have been proposed such as surface coils [33], volume coils [34, 35], and microstrip arrays [36].

In [37], a centrally-fed microstrip line RF coil utilizes capacitive termination has been proposed. This RF coil has demonstrated high quality factor as well as SNR. Meanders at both ends of this RF coil have been added to improve the penetration characteristic and to enhance decoupling [38]. In order to reduce the specific absorption ratio (SAR), the meanders have been loaded by dielectric materials [39]. More properties concerning this RF coil have been reported in [40].

III.2. Materials and methods

The proposed multi-tunable microstrip transmission line RF coil is shown in Figure 1(a). This RF coil has been upgraded from the one that already has been used in several applications, which concentrate only on ^{1}H MR imaging [41, 42]. It consists of two conductors printed on FR-4 substrate (ε_r= 4.4, tan δ= 0.02) of 0.5 mm thickness, with dimensions 250 × 100 mm^2. A ground plane is placed behind the conductors with 20 mm air gap separation. The width of each conductor is 15 mm and for the copper lines within the meanders at both ends of the coil is 2 mm. A homogeneous phantom (ε_r=45.3, σ= 0.8 S/m) with dimensions 600×90×370 mm^3 is located at a distance of 200 mm above the coil. The proposed RF coil makes use of a microfluidically tunable RF capacitor (µTC) to tune between the resonant frequencies of X-nuclei shown in Table 1. Two capacitors have been used to terminate both ends of the RF coil. This capacitor has been designed to have 23 interleaved plates with long microfluidic channel as shown in Figure 1(b). A large tuning range of capacitance has been obtained by inserting fluid with high dielectric constant in these channels and precise control of capacitance has been achieved by controlling the position of this fluid between the metallic plates.

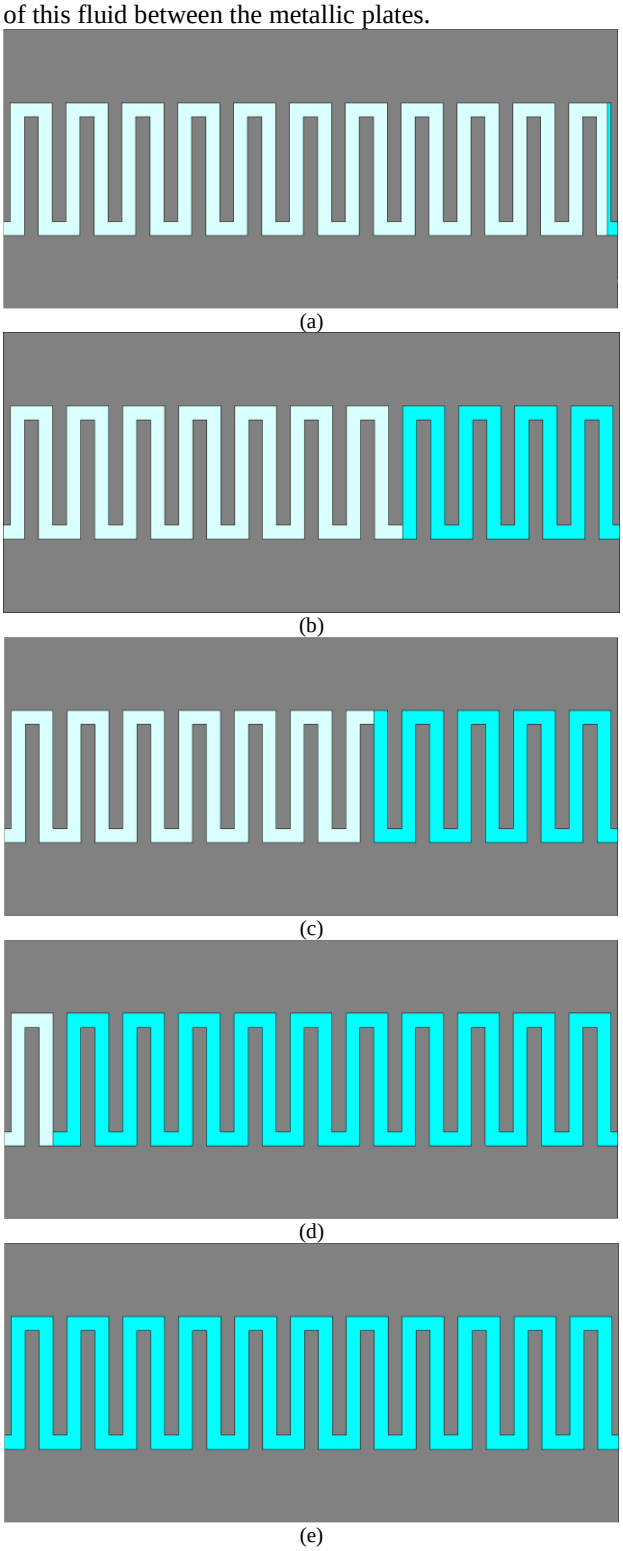

Fig. 2. Fluid positions in channel. (a) ^{1}H, (b) ^{31}P, (c) ^{7}Li, (d) ^{23} Na, (e) ^{13}C.

The SU-8 cover layer, which support some microwave properties [43], has been used with very small thickness

(0.02 mm). The BR33 substrate has been used as mechanical/electrical support.

A parallel plate capacitor is discussed in [44], and the capacitance can be calculated by the following equation:

$$C = (n\text{-}1) \times \textit{capacitance of one pair of plates}$$

$$= (n-1) \times \varepsilon_0 \varepsilon_r \frac{A}{d} \quad (1)$$

where "ε_o" is the absolute permittivity of free space, "ε_r" is the relative permittivity of dielectric medium, "A" is the area of each plate in m^2, "*d*" is the distance between two adjacent parallel plates and "*n*" is the number of interleaved plates. However, we can't rely on this formula for accurate calculation of capacitance since our capacitor has a cover layer and a substrate which leads to a shifting in capacitance. Accurate capacitance values have been obtained by using CST Microwave Studio (CST AG, Darmstadt, Germany) and the calculation method that has been followed can be summarized as follows: the RF coil has been terminated with (µTC) filled totally with deionized (DI) water (ε_r = 80) and the obtained resonant frequency has been compared with the same RF coil terminated with lumped element capacitor instead. By tuning this capacitor to reach the same resonant frequency, the capacitance of (µTC) will be known. The similar procedure has been done by filling the channel of (µTC) with vacuum. Once we have these two capacitance values, we can calculate the total capacitance of the capacitor for any fluid position inside the channel by making use of the following equation:

$$C_t = C_{vacuum} + C_{DI\text{-}water}$$

$$= \frac{1.575 \times a}{4.4} + \frac{48.7 \times (4.4\text{-}a)}{4.4} \quad (2)$$

where "*a*" is the distance of the channel in vacuum as shown in Figure 1(b). The light color in the channel represents the vacuum whereas the dark color represents the fluid. The capacitance of the capacitor in vacuum is equal to 1.575 pF where as the value is equal to 48.7 pF when it is fully filled with DI-water. This capacitor can be modelled as two capacitors connected in series: capacitor filled with vacuum and capacitor filled with fluid. The next step is to calculate the values of "*a*" for all x-nuclei frequencies. This has been done by calculating the capacitance of the lumped capacitor for each frequency using CST and then substitute this value in Equation 2. The values of "a" for all x-nuclei frequencies have been calculated and registered in Table 2. We note that the capacitor value increases as the fluid starts to fill the capacitor channel gradually. Furthermore, the capacitor offers a wide range of capacitance tuning which extends between C_{min}= 1.76 pF and C_{max}= 48.7 pF.

Figure 2 shows five µTCs with different fluid positions in channel for all x-nuclei frequencies.

TABLE II
THE CORRESPONDING CAPACITANCES FOR DIFFERENT X-NUCLEI FREQUENCIES.

Nucleus	**^{1}H**	**^{31}P**	**^{7}Li**	**^{23}Na**	**^{13}C**
Ct(pF)	1.76	18.40	20.10	45.00	48.70
C_{vacuum} (pF)	1.57	1.00	0.96	0.13	0.00
$C_{DI\text{-}water}$ (pF)	0.19	17.40	19.10	44.90	48.70
a (mm)	4.38	2.83	2.67	0.35	0.00

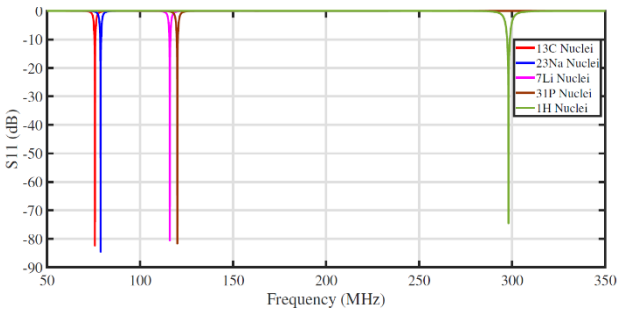

Fig. 3. S11 parameter for different x-nuclei frequencies.

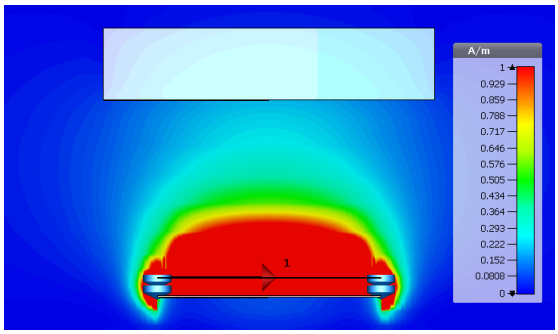

(a) Simulated |H| field in a mid-saggital section.

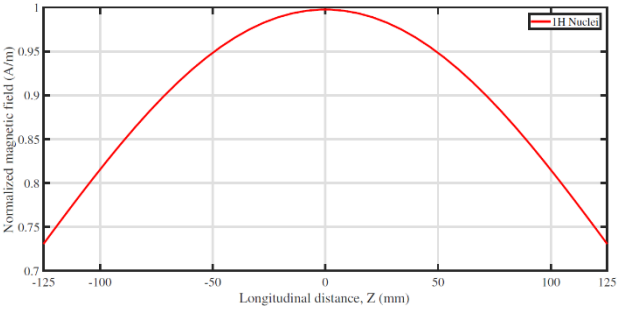

(b) Simulated |H| field, 20mm above the bottom of the phantom.

Fig. 4. Simulated |H| field by using µTC after tuning to ^{1}H frequency.

III.3. Results and discussion

Figure 3 shows the obtained return loss (dB) for different positions of the fluid in the µTC channel. We observe that the maximum resonant frequency (298 MHz) occurres once the capacitance channel is almost empty. When the DI-water starts to be inserted in the capacitor channel, the

resonant frequency decreases until it has fully filled and the resonant frequency reaches the lowest value (75 MHz). The shifting in resonant frequency is not only the resulting effect of inserting the DI-water in the capacitor channel. Indeed, the Q-factor of the RF coil is also degraded as shown in Table 3. The Q-factor has been calculated from the -3dB points of the S11 curve after a matching network. This degradation of Q-factor is affected by the performance of the capacitor. In [45] a detailed study has been done to analyse the performance of microfluidically tuned capacitor. This study demonstrates a degradation of Q-factor of the capacitor with DI-water penetration in capacitor channel. Figure 4(a) shows the magnitude of H-field in a mid-sagittal section for 0.5 W input power after tuning to ^{1}H frequency. We notice that the H-field distribution is focused in the direction of the phantom and decays at the ends of the RF coil. This leads to less radiation loss and increases the transmit sensitivity of the coil on the near side of the phantom. Figure 4(b) shows homogeneous distribution of magnetic field 20 mm inside the phantom along the longitudinal distance of the coil. A similar magnetic field distributions have been obtained in-terms of homogeneity for all other x-nuclei frequencies as seen in Figure 5. However, the magnitude of magnetic field decreases for lower resonant frequencies. This can be justified by comparing the physical length of the RF coil that has been already used in our simulation design and the physical length that should be used to design the RF coil without using additional reactive elements for adjusting the electrical length. This effect is found in dipole antenna. If the gain is calculated at resonant frequency using the corresponding physical length without using reactive load and at lower resonant frequency by using reactive load, the degradation in gain will be observed. One solution to compensate for this degradation is to drive the RF coil by higher excitation signal.

TABLE III RF COIL Q-FACTOR FOR DIFFERENT X-NUCLEI.

Nucleus	**^{1}H**	**^{31}P**	**^{7}Li**	**^{23}Na**	**^{13}C**
3dB Bandwidth (MHz)	4.5	1.9	1.8	1.6	1.7
Q-factor	66	63	63	46	45

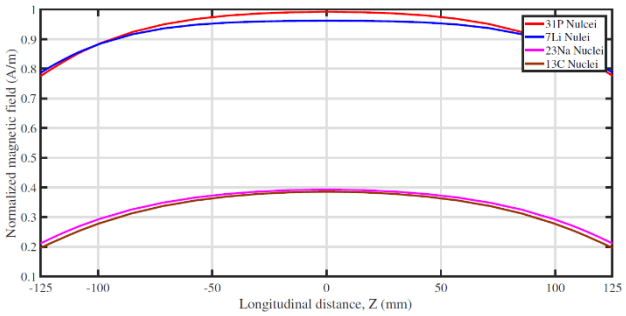

Fig. 5. Simulated |H| field, 20mm above the bottom of the phantom for different x-nuclei frequencies.

IV. Conclusion

A new RF coil tuning method using microfluidically tunable RF capacitor has been investigated to design a multi-tunable microstrip transmission line RF coil. By this capacitor, a range of 47 pF capacitance can be achieved such as to be useful for the most important X-nuclei at 7T (from f_{min}= 75 MHz to f_{max}= 298 MHz). This method can be used for other RF functions, for example, to match the RF coil input impedance to 50 ohm. In order to utilize and integrate this coil to the MRI scanner hardware, a transmit-receive (TR) switch compatible for multi-tuned RF-coil has to be developed, and this is the potential future work.

Acknowledgements

This work has been done at the Applied Science Private University, Amman, Jordan, faculty of engineering, department of Electrical Engineering. The author would like to thank this university for their strong support to this work.

References

[1] *R. Ouwerkerk, K. B. Bleich, J. S. Gillen, M. G. Pomper, and P. A. Bottomley, "Tissue sodium concentration in human brain tumors as measured with ^{23}Na MR Imaging," Radiology, vol. 227, no. 2, pp. 529–537, 2003.*

[2] *R. Ouwerkerk, M. A. Jacobs, K. J. Macura, A. C. Wolff, V. Stearns, S. D. Mezban, N. F. Khouri, D. A. Bluemke, and P. A. Bottomley, "Elevated tissue sodium concentration in malignant breast lesions detected with non-invasive 23Na MRI," Breast cancer research and treatment, vol. 106, no. 2, pp. 151–160, 2007.*

[3] *K. R. Thulborn, D. Davis, J. Snyder, H. Yonas, and A. Kassam, "Sodium MR Imaging of acute and subacute stroke for assessment of tissue viability," Neuroimaging Clinics, vol. 15, no. 3, pp. 639–653, 2005.*

[4] *E. Mellon, D. Pilkinton, C. Clark, M. Elliott, W. Witschey, A. Borthakur, and R. Reddy, "Sodium MR Imaging detection of mild alzheimer disease: preliminary study," American Journal of Neuroradiology, vol. 30, no. 5, pp. 978–984, 2009.*

[5] *N. Maril, Y. Rosen, G. H. Reynolds, A. Ivanishev, L. Ngo, and R. E. Lenkinski, "Sodium MRI of the human kidney at 3 Tesla," Magnetic Resonance in Medicine: An Official Journal of the International Society for Magnetic Resonance in Medicine, vol. 56, no. 6, pp. 1229–1234, 2006.*

[6] *M. Meyerspeer, S. Robinson, C. I. Nabuurs, T. Scheenen, A. Schoisengeier, E. Unger, G. J. Kemp, and E. Moser, "Comparing localized and nonlocalized dynamic 31P magnetic resonance spectroscopy in exercising muscle at 7T," Magnetic resonance in medicine, vol. 68, no. 6, pp. 1713–1723, 2012.*

[7] *D. L. Rothman, I. Magnusson, L. D. Katz, R. G. Shulman, and G. I. Shulman, "Quantitation of hepatic glycogenolysis and gluconeogenesis in fasting humans with 13C NMR," Science, vol. 254, no. 5031, pp. 573–576, 1991.*

[8] *E. M. Haacke, R. W. Brown, M. R. Thompson, R. Venkatesan et al., Magnetic resonance imaging: physical principles and sequence design. Wiley-Liss New York:, 1999, vol. 82.*

[9] A. M. Babsky, S. Topper, H. Zhang, Y. Gao, J. R. James, S. K. Hekmatyar, and N. Bansal, "Evaluation of extraand intracellular apparent diffusion coefficient of sodium in rat skeletal muscle: effects of prolonged ischemia," Magnetic Resonance in Medicine: An Official Journal of the International Society for Magnetic Resonance inMedicine, vol. 59, no. 3, pp. 485–491, 2008.

[10] M. S. Hussain, R. W. Stobbe, Y. A. Bhagat, D. Emery, K. S. Butcher, D. Manawadu, N. Rizvi, P. Maheshwari, J. Scozzafava, A. Shuaib et al., "Sodium imaging intensity increases with time after human ischemic stroke," Annals of Neurology: Official Journal of the American Neurological Association and the Child Neurology Society, vol. 66, no. 1, pp. 55–62, 2009.

[11] S. Trattnig, G. H. Welsch, V. Juras, P. Szomolanyi, M. E. Mayerhoefer, D. Stelzeneder, T. C. Mamisch, O. Bieri, K. Scheffler, and ˇ S. Zb`y, "23Na MR imaging at 7 T after knee matrix–associated autologous chondrocyte transplantation preliminary results," Radiology, vol. 257, no. 1, pp. 175–184, 2010.

[12] R. Gruetter, G. Adriany, I.-Y. Choi, P.-G. Henry, H. Lei, and G. O¨ z, "Localized in vivo 13C NMR spectroscopy of the brain," NMR in Biomedicine: An International Journal Devoted to the Development and Application of Magnetic Resonance In Vivo, vol. 16, no. 6-7, pp. 313–338, 2003.

[13] P.-G. Henry, I. Tk´a˘c, and R. Gruetter, "1H-localized broadband 13C NMR spectroscopy of the rat brain in vivo at 9.4 T," Magnetic Resonance in Medicine: An Official Journal of the International Society for Magnetic Resonance in Medicine, vol. 50, no. 4, pp. 684–692, 2003.

[14] H. P. Hetherington, J. H. Kim, J. W. Pan, and D. D. Spencer, "1H and 31P spectroscopic imaging of epilepsy: spectroscopic and histologic correlations," Epilepsia, vol. 45, pp. 17–23, 2004.

[15] F. Wetterling, M. H¨ogler, U. Molkenthin, S. Junge, L. Gallagher, I. M. Macrae, and A. J. Fagan, "The design of a double-tuned two-port surface resonator and its application to in vivo Hydrogen-and Sodium-MRI," Journal of magnetic resonance, vol. 217, pp. 10–18, 2012.

[16] S.-D. Han, P. Heo, H.-J. Kim, H. Song, D. Kim, J.-H. Seo, Y. Ryu, Y. Noh, and K.-N. Kim, "Double-layered dual-tuned RF coil using frequency-selectable PIN-diode control at 7-T MRI," Concepts in Magnetic Resonance Part B: Magnetic Resonance Engineering, vol. 47, no. 4, p. e21363, 2017.

[17] L. T. Muftuler, G. Gulsen, K. D. Sezen, and O. Nalcioglu, "Automatic tuned MRI RF coil for multinuclear imaging of small animals at 3T," Journal of Magnetic Resonance, vol. 155, no. 1, pp. 39–44, 2002.

[18] D. T. McCormick, Z. Li, and N. Tien, "Dielectric fluid immersed MEMS tunable capacitors," in IEEE MTT-S International Microwave Symposium Digest, 2003, vol. 1. IEEE, 2003, pp. 495–498.

[19] T. Platt, A. Korzowski, R. Umathum, and P. Bachert, "Double-resonant 13c/1h coil system for 1H 13C in vivo NMR spectroscopy on a 7T whole-body MR tomography," 22nd Proc. Intl. Soc. MRM, p. 1346, 2014.

[20] G. Isaac, M. D. Schnall, R. E. Lenkinski, and K. Vogele, "A design for a double-tuned birdcage coil for use in an integrated MRI/MRS examination," Journal of Magnetic Resonance (1969), vol. 89, no. 1, pp. 41–50, 1990.

[21] G. X. Shen, F. E. Boada, and K. R. Thulborn, "Dual-frequency, dual-quadrature, birdcage RF coil design with identical B1 pattern for sodium and proton imaging of the human brain at 1.5 T," Magnetic resonance in medicine, vol. 38, no. 5, pp. 717–725, 1997.

[22] C.-H. Choi, J. M. Hutchison, and D. J. Lurie, "Design and construction of an actively frequency-switchable RF coil for field-dependent Magnetisation Transfer Contrast MRI with fast field-cycling," Journal of Magnetic Resonance, vol. 207, no. 1, pp. 134–139, 2010.

[23] S. Ha, M. J. Hamamura, O. Nalcioglu, and L. T. Muftuler, "A PIN diode controlled dual-tuned MRI RF coil and phased array for multi nuclear imaging," Physics in Medicine & Biology, vol. 55, no. 9, p. 2589, 2010.

[24] M. Meyerspeer, E. S. Roig, R. Gruetter, and A.W. Magill, "An improved trap design for decoupling multinuclear RF coils," Magnetic resonance in medicine, vol. 72, no. 2, pp. 584–590, 2014.

[25] M. Alecci, S. Romanzetti, J. Kaffanke, A. Celik, H.Wegener, and N. Shah, "Practical design of a 4 Tesla doubletuned RF surface coil for interleaved 1H and 23Na MRI of rat brain," Journal of Magnetic Resonance, vol. 181, no. 2, pp. 203–211, 2006.

[26] J. R. Fitzsimmons, B. L. Beck, and H. Ralph Brooker, "Double resonant quadrature birdcage," Magnetic resonance in medicine, vol. 30, no. 1, pp. 107–114, 1993.

[27] Y. Ha, C.-H. Choi, W. A. Worthoff, A. Shymanskaya, M. Sch¨oneck, A. Willuweit, J. Felder, and N. J. Shah, "Design and use of a folded four-ring double-tuned birdcage coil for rat brain sodium imaging at 9.4 T," Journal of Magnetic Resonance, vol. 286, pp. 110–114, 2018.

[28] Y. Pang, Z. Xie, D. Xu, D. A. Kelley, S. J. Nelson, D. B. Vigneron, and X. Zhang, "A dual-tuned quadrature volume coil with mixed _λ/2 and _λ/4 microstrip resonators for multinuclear MRSI at 7 T," Magnetic resonance imaging, vol. 30, no. 2, pp. 290–298, 2012.

[29] O. Rutledge, T. Kwak, P. Cao, and X. Zhang, "Design and test of a double-nuclear RF coil for 1H MRI and 13C MRSI at 7 T," Journal of Magnetic Resonance, vol. 267, pp. 15–21, 2016.

[30] E. Yacoub, A. Shmuel, J. Pfeuffer, P.-F. Van De Moortele, G. Adriany, P. Andersen, J. T. Vaughan, H. Merkle, K. Ugurbil, and X. Hu, "Imaging brain function in humans at 7 Tesla," Magnetic Resonance in Medicine: An Official Journal of the International Society for Magnetic Resonance in Medicine, vol. 45, no. 4, pp. 588–594, 2001.

[31] J. T. Vaughan, M. Garwood, C. Collins, W. Liu, L. DelaBarre, G. Adriany, P. Andersen, H. Merkle, R. Goebel, M. Smith et al., "7T vs. 4T: RF power, homogeneity, and signal-to-noise comparison in head images," Magnetic Resonance in Medicine: An Official Journal of the International Society for Magnetic Resonance in Medicine, vol. 46, no. 1, pp. 24–30, 2001.

[32] C. M. Collins and M. B. Smith, "Signal-to-noise ratio and absorbed power as functions of main magnetic field strength, and definition of 90_ RF pulse for the head in the birdcage coil," Magnetic Resonance in Medicine: An Official Journal of the International Society for Magnetic Resonance in Medicine, vol. 45, no. 4, pp. 684–691, 2001.

[33] X. Zhang, K. Ugurbil, and W. Chen, "Microstrip RF surface coil design for extremely high-field MRI and spectroscopy," Magnetic Resonance in Medicine: An Official Journal of the International Society for Magnetic Resonance in Medicine, vol. 46, no. 3, pp. 443–450, 2001.

[34] X. Zhang, K. Ugurbil, and Chen, "A microstrip transmission line volume coil for human head MR imaging at 4 T," Journal of Magnetic Resonance, vol. 161, no. 2, pp. 242–251, 2003.

[35] Y. Pang, Z. Xie, Y. Li, D. Xu, D. Vigneron, and X. Zhang, "Resonant mode reduction in radiofrequency volume coils for ultrahigh field magnetic resonance imaging," Materials, vol. 4, no. 8, pp. 1333–1344, 2011.

[36] R. F. Lee, C. R.Westgate, R. G.Weiss, D. C. Newman, and P. A. Bottomley, "Planar strip array (PSA) for MRI," Magnetic Resonance in Medicine: An Official Journal of the International

Society for Magnetic Resonance in Medicine, vol. 45, no. 4, pp. 673–683, 2001.

[37] *D. O. Brunner, N. De Zanche, J. Froehlich, D. Baumann, and K. Pruessmann, "A symmetrically fed microstrip coil array for 7T," 15th Proc. Intl. Soc. MRM, p. 448, 2007.*

[38] *S. Orzada, A. Bahr, and T. Bolz, "A novel 7 T microstrip element using meanders to enhance decoupling,"Meander, vol. 1, no. 36, pp. 10–7, 2008.*

[39] *G. Saleh, K. Solbach, A. Rennings, and Z. Chen, "SAR reduction for dipole RF coil element at 7 Tesla by using dielectric overlay," in 2012 Loughborough Antennas & Propagation Conference (LAPC). IEEE, 2012, pp. 1–3.*

[40] *A. Abuelhaija, K. Solbach, and S. Orzada, "Comprehensive study on coupled meandered microstrip line RF coil elements for 7-Tesla magnetic resonance imaging," in 2015 9th European Conference on Antennas and Propagation (EuCAP). IEEE, 2015, pp. 1–5.*

[41] *[41] S. Orzada, A. K. Bitz, S. Johst, M. Gratz, M. N. V¨olker, O. Kraff, A. Abuelhaija, T. M. Fiedler, K. Solbach, H. H. Quick et al., "Analysis of an integrated 8-Channel Tx/Rx body array for use as a body coil in 7-Tesla MRI," Frontiers in Physics, vol. 5, p. 17, 2017.*

[42] *S. Orzada, A. Bitz, M. Gratz, S. Johst, S. Shooshtary, M. Voelker, S. Rietsch, M. Fl¨oser, A. Abuelhaija, M. Oehmigen et al., "A 32-channel transmit system add-on for 7 Tesla body imaging," in Proc. Intl. Soc. Mag. Reson. Med, vol. 25, 2017, p. 1219.*

[43] *H. Habbachi, H. Boussetta, A. Boukabache, K. A. Kallala, P. Pons, and K. Besbes, "Study of a tunable MEMS capacitor: influence of fluids," Electronics Letters, vol. 53, no. 2, pp. pp.72–73, Nov. 2016. [Online]. Available: https://hal.laas.fr/hal-01415341*

[44] *A. Chakrabarti, S. Nath, and C. K. Chanda, Basic Electrical Engineering. Tata McGraw-Hill, 2009.*

[45] *N. Habbachi, A. Boukabache, H. Boussetta, P. Pons, M. A. Kallala, and K. Besbes, "Modeling of microfluidically tuned capacitor for RF applications," in 2018 15th International Multi-Conference on Systems, Signals & Devices (SSD). IEEE, 2018, pp. 816–820.*

AUTHORS' INFORMATION

[1]Department of Electrical Engineering, Applied Science Private University, Amman, Jordan.

[2]Telecommunication Engineering Department, Arab American University, Jenin, Palestine.

[3]Institute of Digital Signal Processing, Duisburg-Essen University, Germany.

Ashraf Abuelhaija received the B.Sc. degree in communications and electronics engineering from Applied Science Private University, Amman, Jordan, in 2007, and the master's and Ph.D. degrees in electrical engineering from the University of Duisburg-Essen in 2010 and 2016, respectively. From 2012 to 2014, he was a Research Assistant with the Erwin L. Hahn Institute for Magnetic Resonance Imaging, Essen. From 2014 to 2016, he was a Research Assistant with the Department of Microwave and RF Technology, University of Duisburg-Essen. He is currently an Assistant Professor with the Department of Electrical Engineering, Applied Science Private University. His research interests are in the area of antennas and RF technology.

